

Analysis of fiber-reinforced elastomeric isolators under pure “warping”

Seval Pinarbasi*¹ and Yalcin Mengi²

¹Department of Civil Engineering, Kocaeli University, Kocaeli 41380, Turkey

²Department of Engineering Sciences, Middle East Technical University, Ankara 06531, Turkey

(Received March 12, 2016, Revised August 12, 2016, Accepted August 23, 2016)

Abstract. As a relatively new type of multi-layered rubber-based seismic isolators, fiber-reinforced elastomeric isolators (FREIs) are composed of several thin rubber layers reinforced with flexible fiber sheets. Limited analytical studies in literature have pointed out that “warping” (distortion) of reinforcing sheets has significant influence on buckling behavior of FREIs. However, none of these studies, to the best knowledge of authors, has investigated their warping behavior, thoroughly. This study aims to investigate, in detail, the warping behavior of strip-shaped FREIs by deriving advanced analytical solutions without utilizing the commonly used “pressure”, incompressibility, inextensibility and the “linear axial displacement variation through the thickness” assumptions. Studies show that the warping behavior of FREIs mainly depends on the (i) aspect ratio (shape factor) of the interior elastomer layers, (ii) Poisson’s ratio of the elastomer and (iii) extensibility of the fiber sheets. The basic assumptions of the “pressure” method as well as the commonly used incompressibility assumption are valid only for isolators with relatively large shape factors, strictly incompressible elastomeric material and nearly inextensible fiber reinforcement.

Keywords: bearing; buckling; distortion; elastomeric isolator; fiber-reinforced isolator; rubber; seismic isolation; warping

1. Introduction

Earlier studies (e.g., Gent and Lindley 1959) have showed that the compression/bending stiffness of an elastic layer bonded to reinforcing sheets may be several orders of magnitude greater than that of the corresponding unbonded layer while the effect of the bonded faces to the shear behavior of the layer is almost negligible unless the layer thickness and/or the applied loads are considerably large. This is an important property in view of that the resistance of a soft elastic layer to compression and bending can be increased, without compromising from its flexibility in shear, by bonding it to reinforcing plates at its top and bottom faces.

Composed of several elastomer layers bonded to steel reinforcing sheets, steel-laminated elastomeric isolators have been developed using this favorable mechanical property of “bonded” elastic layers. Steel-reinforced elastomeric isolators are widely used in many engineering applications to isolate the structural/mechanical systems from the detrimental effects of different types of vibrations (Kelly 1997, Kelly and Konstantinidis 2011). Since the stiffness ratio for a typical interior steel-rubber unit is significantly large, steel plates are usually assumed to be “rigid” unless they are too thin or the applied loads are too large. In an effort to develop light-weight, low-cost isolators to be used in developing countries, Kelly (1994) sought the minimum steel plate thickness that ensures their “rigidity”

and studied the possibility and viability of using thinner steel plates or more flexible reinforcement. He found out that the reinforcement flexibility, which causes “warping” (distortional) deformations in the reinforcing sheets, has significant effect on buckling behavior of a multi-layered elastomeric isolator and stated that “for the typical range of sizes of isolators for buildings, the reduction in buckling load from the completely rigid plate case to the completely flexible plate case is from 25% to 50%”. He also indicated that “3.18 mm (1/8 in.) thick steel plates have almost the same buckling load as the completely rigid case and 0.79 mm (1/32 in.) thick steel plates have almost the same buckling load as the completely flexible case”. Kelly (1994) also highlighted that, although it analytically appears to be possible to reduce the thickness of steel plates significantly, it may not always be possible to do so in practice since these plates have to be sand-blasted before being bonded to the elastomer, which can easily damage them if they are too thin. Thus, as proposed by Kelly (1999), it seems to be more practical and feasible to reduce the weight and cost of the bearings by replacing steel reinforcement with “equivalent” fiber reinforcement. In literature, many studies have been conducted on fiber-reinforced elastomeric isolators (e.g., Kelly and Takhirov 2001, Kelly 2002, Tsai and Kelly 2005, Pinarbasi and Mengi 2008, Pinarbasi, Mengi *et al.* 2008, Toopchi-Nezhad, Tait *et al.* 2011, Pinarbasi and Okay 2011, Kelly and Calabrese 2012, Angeli, Russo *et al.* 2013, Osgooei, Tait *et al.* 2014, Toopchi-Nezhad 2014, Osgooei, Engelen *et al.* 2015, Yasser and Tait 2015). These studies have verified the viability of the use of fiber sheets as reinforcing agents in multi-layered seismic isolators.

*Corresponding author, Associate Professor
E-mail: sevalp@gmail.com

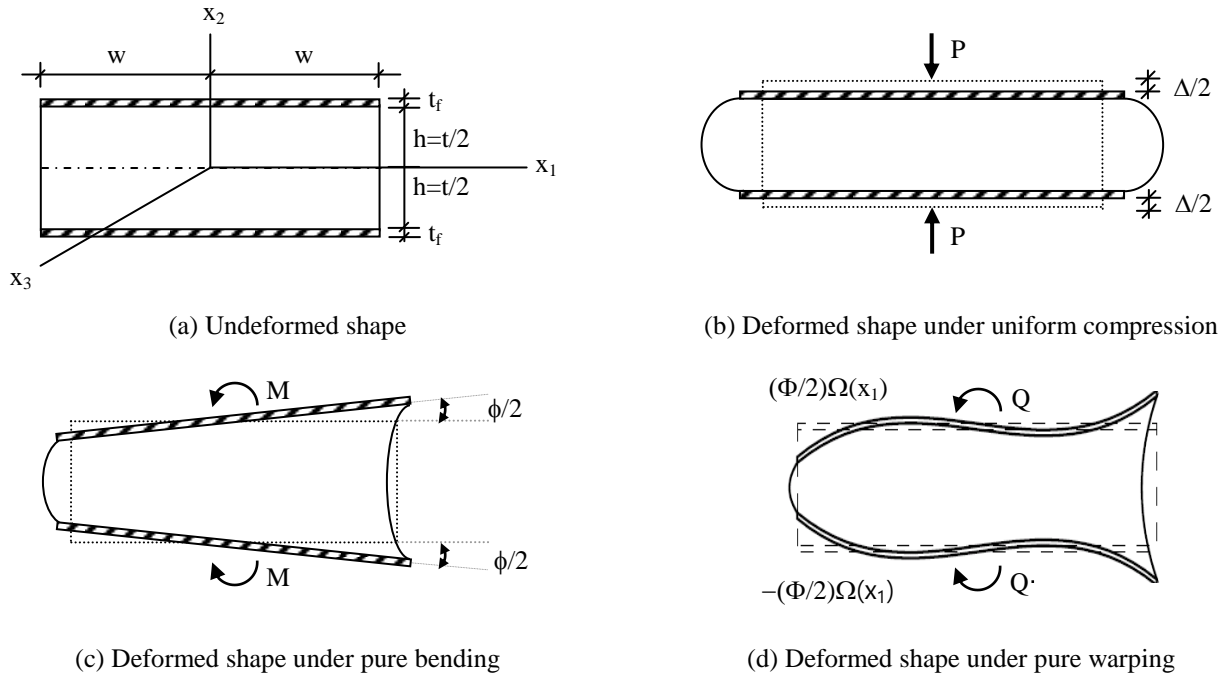


Fig. 1 An elastic layer bonded to flexible reinforcements under uniform compression, pure bending and pure warping

The compressive or bending behavior of a multi-layered elastomeric isolator can realistically be studied by analyzing its typical interior “bonded” elastomer layer (Kelly and Konstantinidis 2011). As reviewed in Pinarbasi, Akyuz *et al.* (2006) in detail, in the last century, many researchers have studied the behavior of rigidly-bonded (i.e., steel-reinforced) elastic layers. The earliest studies on this subject (e.g., Gent and Lindley 1959) put forward three fundamental assumptions on displacement and stress patterns in a bonded elastic layer: (i) initially vertical lateral surfaces take a parabolic shape in the deformed configuration, (ii) horizontal plane sections remain plane after deformation, (iii) state of stress at any point in the material is dominated by the hydrostatic pressure. Due to the last, i.e., “pressure” assumption, the formulations developed using these fundamental assumptions are commonly named, in literature, as the “pressure method”.

With the proposal of using fiber-reinforcement in seismic isolators, analytical studies on bonded elastic layers are directed towards elastic layers bonded to flexible reinforcements. The effect of reinforcement flexibility on compressive and bending behavior of fiber-reinforced elastomeric isolators has been studied in various works (e.g., Kelly 1999, Kelly and Takhirov 2001, Kelly 2002, Tsai and Kelly 2005, Tsai 2007, Pinarbasi and Mengi 2008, Pinarbasi, Mengi *et al.* 2008, Pinarbasi and Okay 2011, Kelly and Konstantinidis 2011, Angeli, Russo *et al.* 2013). Similar to the steel-reinforced case, most of these analytical studies are conducted on an individual elastomer layer bonded to flexible fiber-reinforced sheets. There is an important difference, however, in the analyses of these two cases: while in the analysis of a steel-reinforced layer, the reinforcement is assumed to be rigid both in extension and flexure, in the analysis of a fiber-reinforced layer, it is assumed to be “flexible in extension but completely without

flexure rigidity” (Kelly 2002). Earlier studies on fiber-reinforced layers (Fig. 1(a)) have mostly been concentrated on investigating the layer behavior under uniform compression (Fig. 1(b)) and/or “pure” bending, i.e., bending without warping (Fig. 1(c)). The works by Kelly (1994) and Tsai and Kelly (2005) are different from the others in that they included in their formulations “pure” warping (distortional deformations) of the reinforcing sheets (Fig. 1(d)). Ignoring the extensibility of the reinforcement and using the pressure approach, Kelly (1994) derived a closed-form expression for effective “warping modulus” of strip-shaped bonded elastic layers. Following a similar approach and including the extensibility of the reinforcing sheets, Tsai and Kelly (2005) obtained a more general expression for the warping modulus. However, neither Kelly (1994), nor Tsai and Kelly (2005) investigated the warping behavior of the layer thoroughly. It is to be noted that their formulations are based on three fundamental assumptions of the pressure method as well as the incompressibility assumption.

Our recent studies (Pinarbasi, Akyuz *et al.* 2006, Pinarbasi and Mengi 2008, Pinarbasi, Mengi *et al.* 2008) showed that it is possible to eliminate most of these assumptions by using the higher order theory developed by Mengi (1980). The aim of this study is to investigate, in detail, the warping behavior of elastomeric layers bonded to flexible reinforcements, thus the warping behavior of multi-layered fiber-reinforced elastomeric isolators, by using the advanced solutions derived for strip-shaped layers from this higher order theory. The application of the theory to the associated warping problem (Fig. 1(d)) has already been shown in Pinarbasi and Mengi (2008), where the governing equations of the problem were solved for strip-shaped layers by using the zeroth order theory. For a comprehensive study on warping behavior, particularly for

a detailed analysis on stress distributions, it is more convenient to increase the order of the theory. Our earlier studies with higher order theories have indicated that while it is not possible to obtain closed-form solutions to the problem when second or higher order theories are used due to highly nonlinear and coupled forms of the governing equations, it is possible to do so when the first order theory is used in the formulation. In this paper, these analytical solutions are derived first. Free from the commonly used incompressibility, inextensibility, “pressure” and the “linear variation of axial displacement through the thickness” assumptions, these advanced solutions become handy tools for investigating warping behavior of fiber-reinforced strips thoroughly.

2. Analysis of strip-shaped fiber-reinforced elastomeric isolators under pure warping

2.1 Review of the theory used in the study

The analytical formulation used in this study to investigate the warping behavior of a strip-shaped fiber-reinforced elastomeric isolator, in other words, warping behavior of its typical interior elastomer layer bonded to fiber reinforcement at its top and bottom faces, has been developed from an approximate theory proposed by Mengi (1980), which is reviewed shortly in this section to introduce the notation.

Consider an elastic and isotropic layer with uniform thickness of $2h$ referred to a Cartesian coordinate system (x_1 x_2 x_3), where the x_1x_3 plane coincides the mid-plane of the layer, as shown in Fig. 1(a). The theory by Mengi (1980) contains two types of field variables: (i) “generalized variables” representing the weighted averages of displacements (u_i , $i=1-3$) and stresses (τ_{ij} , $i,j=1-3$) over the thickness of the layer, denoted respectively by u_i^n and τ_{ij}^n where $n=0-m$ for the m th order theory, and (ii) “face variables” representing the components of displacements and tractions on the lateral faces of the layer, denoted, respectively: $u_i^\pm = u_i|_{x_2=\pm h}$ and $\tau_{2i}^\pm = \tau_{2i}|_{x_2=\pm h}$. In the development of the theory, a set of distribution functions $\phi_n(\bar{x}_2)$ ($n=0,1,2,\dots$; $\bar{x}_2 = x_2/h$) is chosen. For the m th order theory, the elements ϕ_n ($n=0$ to $(m+2)$) are retained in the set.

There are basically two sets of equations. The “weighted averages of elasticity equations” are obtained by applying the operator $L^n = \frac{1}{2h} \int_{-h}^{+h} (\cdot) \phi_n dx_2$, with ϕ_n ($n=0-m$), to the equilibrium and constitutive equations of linear elasticity. The “constitutive equations for face variables” are obtained through the expansion of displacements in terms of the distribution functions as $u_i = \sum_{k=0}^{m+2} a_k^i \phi_k$ (where a_k^i are some constants) and using it in the exact constitutive equations of tractions on flat faces of the layer.

Written in indicial notation, the fundamental equations of linear elasticity, namely, equilibrium (in the absence of

body forces) and constitutive equations are

$$\partial_j \tau_{ji} = 0 \quad (i,j=1-3) \quad (1)$$

$$\tau_{ij} = \mu (\partial_i u_j + \partial_j u_i) + \delta_{ij} \lambda \partial_k u_k \quad (i,j=1-3) \quad (2)$$

where λ , μ are Lamé’s constants and δ_{ij} is the Kronecker delta. In writing Eqs. (1) and (2), the summation convention is used, thus any repeated index indicates summation over its range. Moreover, ∂_i implies partial differentiation with respect to x_i .

The weighted averages of fundamental equations are established by applying the operator $L^n = \frac{1}{2h} \int_{-h}^{+h} (\cdot) \phi_n dx_2$

with $n=0-m$ to Eqs. (1) and (2), which gives

$$\partial_1 \tau_{1i}^n + \partial_3 \tau_{3i}^n + (R_i^n - \bar{\tau}_{2i}^n) = 0 \quad (i=1-3, n=0-m) \quad (3)$$

where

$$R_i^n = \frac{\hat{R}_i^n \phi_n(1)}{2h} \quad \text{where} \quad \hat{R}_i^n = \begin{cases} R_i^- = \tau_{2i}^+ - \tau_{2i}^- & \text{for even } n \\ R_i^+ = \tau_{2i}^+ + \tau_{2i}^- & \text{for odd } n \end{cases} \quad \text{with} \quad (4)$$

$$\tau_{2i}^\pm = \tau_{2i}|_{x_2=\pm h}$$

$$\tau_{ji}^n = L^n \tau_{ji} \quad , \quad (i=1,3), \quad \bar{\tau}_{2i}^n = \bar{L}^n \tau_{2i} \quad \text{with}$$

$$\bar{L}^n = \frac{1}{2h} \int_{-h}^h (\cdot) \frac{d\phi_n}{dx_2} dx_2 \quad (5)$$

and

$$\begin{aligned} \tau_{11}^n &= \alpha \partial_1 u_1^n + \lambda \partial_3 u_3^n + \lambda (S_2^n - \bar{u}_2^n) \\ \tau_{22}^n &= \lambda \partial_1 u_1^n + \lambda \partial_3 u_3^n + \alpha (S_2^n - \bar{u}_2^n) \\ \tau_{33}^n &= \alpha \partial_3 u_3^n + \lambda \partial_1 u_1^n + \lambda (S_2^n - \bar{u}_2^n) \\ \tau_{12}^n &= \mu \partial_1 u_2^n + \mu (S_1^n - \bar{u}_1^n) \end{aligned} \quad (6)$$

$$\tau_{13}^n = \mu \partial_1 u_3^n + \mu \partial_3 u_1^n \quad \tau_{23}^n = \mu \partial_3 u_2^n + \mu (S_3^n - \bar{u}_3^n) \quad (n=0-m)$$

where

$$S_i^n = \frac{\hat{S}_i^n \phi_n(1)}{2h} \quad \text{where} \quad \hat{S}_i^n = \begin{cases} S_i^- = u_i^+ - u_i^- & \text{for even } n \\ S_i^+ = u_i^+ + u_i^- & \text{for odd } n \end{cases} \quad \text{with} \quad (7)$$

$$u_i^\pm = u_i|_{x_2=\pm h}$$

$$u_i^n = L^n u_i \quad \text{and} \quad \bar{u}_i^n = \bar{L}^n u_i \quad (i=1-3)$$

In Eqs. (3)-(7), $\alpha = 2\mu + \lambda$, and $p=m$ and $p'=m-1$ for even m and $p=m-1$ and $p'=m$ for odd m . While deriving Eqs. (3)-(7), the theory assumes that ϕ_n is even function of x_2 for even n , and odd function of x_2 for odd n , and that

$\phi'_n = d\phi_n / d\bar{x}_2$ is related to ϕ_j through some coefficients c_{nj} by $\phi'_n = \sum_{j=0}^m c_{nj} \phi_j$, implying that $\bar{\tau}_{2i}^n$ and \bar{u}_i^n are related to τ_{2i}^n and u_i^n by

$$(\bar{\tau}_{2i}^n, \bar{u}_i^n) = \frac{1}{h} \sum_{j=0}^m c_{nj} (\tau_{2i}^j, u_i^j) \quad (8)$$

For the derivation of the constitutive equations for face variables R_i^\pm , displacements u_i are expanded in terms of ϕ_k ($k=0,1,2,\dots,m+2$) as

$$u_i = \sum_{k=0}^{m+2} a_k^i \phi_k \quad (9)$$

where a_k^i are some coefficients which are functions of x_1 and x_3 . When L^n ($n=0-m$) operator is applied to this expression, one obtains

$$u_i^n = \sum_{k=0}^{m+2} d_{nk} a_k^i \quad \text{where} \quad (10)$$

$$d_{nk} = L^n \phi_k = \frac{1}{2h} \int_{-h}^h \phi_n \phi_k dx_2$$

Assumed properties of ϕ_k lead to the following uncoupled system of equations for the determination of coefficients a_k^i

$$u_i^n = \sum_{k=0,2}^{p+2} d_{nk} a_k^i \quad \text{and} \quad \frac{S_i^+}{2} = \sum_{k=0,2}^{p+2} a_k^i \phi_k(1) \quad (n=0,2,\dots, p) \quad \text{for even } k \quad (11)$$

$$u_i^n = \sum_{k=1,3}^{p+2} d_{nk} a_k^i \quad \text{and} \quad \frac{S_i^-}{2} = \sum_{k=1,3}^{p+2} a_k^i \phi_k(1) \quad (n=1,3,\dots, p) \quad \text{for odd } k$$

where $p=m$ and $p'=m-1$ for even m and $p=m-1$ and $p'=m$ for odd m . From the solutions of above equations, the coefficients a_k^i are determined in terms of u_i^n and S_i^\pm as

$$a_k^i = \sum_{j=0,2}^p f_{kj} u_i^j + f_{k,p+2} S_i^+ \quad \text{for even } k \quad \text{and} \quad (12)$$

$$a_k^i = \sum_{j=1,3}^{p'} f_{kj} u_i^j + f_{k,p'+2} S_i^- \quad \text{for odd } k$$

where the coefficients f_{kj} ($k,j=0-m+2$) may be computed whenever ϕ_n are chosen.

Finally, the constitutive equations for face variables can be obtained by using Eq. (9) in $R_i^\pm = \tau_{2i}^+ \pm \tau_{2i}^-$ with $\tau_{2i} = \mu(\partial_2 u_i + \partial_1 u_2) + \lambda \delta_{i2} \partial_k u_k$, which gives

$$R_i^+ = \mu(\partial_i S_2^+) + \frac{2\mu}{h} \left(\sum_{k=1,3}^p \gamma_k u_i^k + \gamma^- S_i^- \right) \quad (13)$$

$$R_i^- = \mu(\partial_i S_2^-) + \frac{2\mu}{h} \left(\sum_{k=0,2}^p \gamma_k u_i^k + \gamma^+ S_i^+ \right), \quad (i=1,3)$$

$$R_2^+ = \lambda(\partial_1 S_1^+ + \partial_3 S_3^+) + \frac{2\alpha}{h} \left(\sum_{k=1,3}^{p'} \gamma_k u_2^k + \gamma^- S_2^- \right)$$

$$R_2^- = \lambda(\partial_1 S_1^- + \partial_3 S_3^-) + \frac{2\alpha}{h} \left(\sum_{k=0,2}^p \gamma_k u_2^k + \gamma^+ S_2^+ \right)$$

where

$$\gamma_j = \sum_{k=1,3}^{p'+2} f_{kj} \phi'_k(1) \quad \text{for } j=1,3,\dots,p' \quad \text{and}$$

$$\gamma_j = \sum_{k=0,2}^{p+2} f_{kj} \phi'_k(1) \quad \text{for } j=0,2,\dots,p \quad (14)$$

$$\gamma^- = \sum_{k=1,3}^{p'+2} f_{k,p'+2} \phi'_k(1) \quad \text{and}$$

$$\gamma^+ = \sum_{k=0,2}^{p+2} f_{k,p+2} \phi'_k(1)$$

The coefficients c_{nj} and the constants a_k^i , γ_j , γ^\pm of the theory can be determined for any order of the theory whenever the distribution functions ϕ_n are chosen.

2.2 Application of the theory to the warping problem

The theory can easily be applied to the problem illustrated in Fig. 1(d), where a strip-shaped layer whose length is much larger than its width $2w$ and thickness t is subjected to the warping moments Q so that the reinforcing sheets with an equivalent thickness of t_f deform about x_3 axis with a warping shape $(\pm\Phi/2)\Omega(x_1)$. Since such a layer may be approximated in a state of plane strain, $u_3=0$, $u_3^\pm=0$, and u_1 , u_2 and u_1^\pm (stretching of the reinforcing sheets, which is also assumed to be in a state of plane stress, in the direction of "finite" length of the layer) are independent of x_3 . It is also known that, under pure warping, u_2 is antisymmetric whereas u_1 and u_3 are symmetric about the mid-plane of the layer (see Fig. 1(d)). Since the distribution functions are even functions of \bar{x}_2 for even n , and odd functions of \bar{x}_2 for odd n , one has

$$u_1^n = 0 \quad \text{and} \quad \bar{u}_2^n = 0 \quad \text{for odd } n; \quad (15)$$

$$\bar{u}_1^n = 0 \quad \text{and} \quad u_2^n = 0 \quad \text{for even } n$$

Considering that u_1 and u_3 are also symmetric about the mid-plane of the layer, the face displacements can be written in the following form

$$u_1^+ = u_1^- \quad \text{and} \quad u_2^\pm = \pm \frac{\Phi}{2} \Omega(x_1) \quad (16)$$

which leads to

$$S_1^- = S_2^+ = 0, \quad S_1^+ = 2u_1^+ = 2u_1^-, \quad \text{and} \quad (17)$$

$$S_2^- = \Phi\Omega(x_1)$$

Then, with the selection of Legendre's polynomials as the distribution functions, the governing equations of the approximate theory reduce to the following equations for

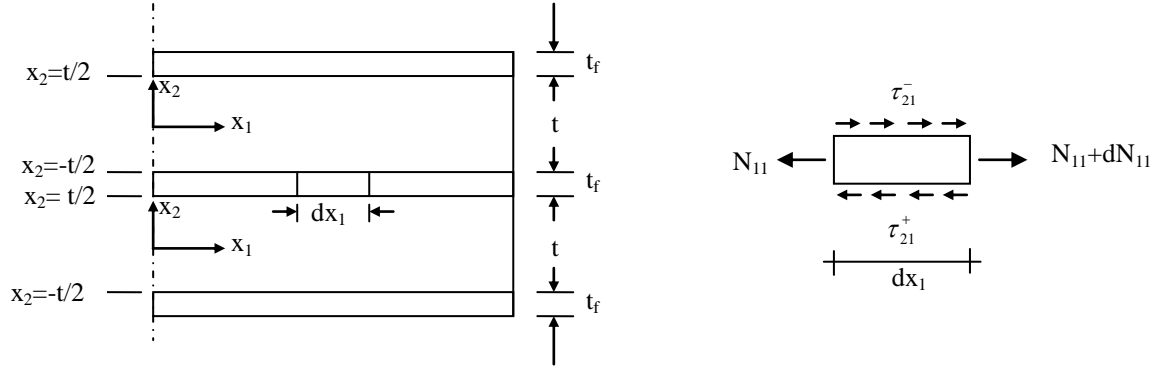


Fig. 2 Forces on an infinitesimal area of a reinforcing sheet bonded to rubber layers at its top/bottom faces

the studied plane strain problem (for details, refer to Pinarbasi and Mengi 2008):

- weighted equilibrium equations

$$\begin{aligned} & \alpha \partial_{11} u_1^n - \lambda \partial_1 \bar{u}_2^n + \frac{4\mu}{t^2} \left(\sum_{k=0,2}^p \gamma_k u_1^k \right) + \frac{8\mu}{t^2} \gamma^+ u_1^+ \\ & + (\lambda + \mu) \frac{\Phi}{t} \partial_1 \Omega = \bar{\tau}_{21}^n \quad \text{for even } n \\ & \mu \partial_{11} u_2^n - \mu \partial_1 \bar{u}_1^n + \frac{4\alpha}{t^2} \left(\sum_{k=1,3}^{p'} \gamma_k u_2^k \right) \\ & + \frac{2}{t} (\mu + \lambda) (\partial_1 u_1^+) + \frac{4\alpha}{t^2} \gamma^- \Phi \Omega = \bar{\tau}_{22}^n \quad \text{for odd } n \end{aligned} \quad (18)$$

- weighted constitutive equations

$$\begin{aligned} & \tau_{12}^n = \mu \partial_1 u_2^n - \mu \bar{u}_1^n + \frac{2\mu}{t} u_1^+ \quad \text{for odd } n \\ & \left. \begin{aligned} \tau_{11}^n &= \alpha \partial_1 u_1^n + \frac{\lambda \Phi}{t} \Omega - \lambda \bar{u}_2^n \\ \tau_{33}^n &= \lambda \partial_1 u_1^n + \frac{\lambda \Phi}{t} \Omega - \lambda \bar{u}_2^n \\ \tau_{22}^n &= \lambda \partial_1 u_1^n + \frac{\alpha \Phi}{t} \Omega - \alpha \bar{u}_2^n \end{aligned} \right\} \quad \text{for even } n \end{aligned} \quad (19)$$

where \bar{u}_i^n and $\bar{\tau}_{2i}^n$ are related to u_i^n and τ_{2i}^n by, in view of Eq. (8)

$$(\bar{u}_i^n, \bar{\tau}_{2i}^n) = \frac{2}{t} \sum_{j=0}^m c_{nj} (u_i^j, \tau_{2i}^j) \quad (20)$$

in which τ_{2i}^j can be expressed in terms of u_i^n and u_1^+ by Eq. (19).

For a monotonically-deformed interior bonded layer, internal forces on an infinitesimal area of a reinforcing sheet bonded to elastic layers at its top and bottom surfaces are illustrated in Fig. 2, where N_{11} is the stretching force per unit length in the x_1 direction and τ_{21}^+ and τ_{21}^- are bonding shear stresses. As shown by Pinarbasi and Mengi (2008), by using the elastic stress strain relation for the reinforcement deformation, the additional equation coming from the reinforcement equilibrium can be obtained as follows

$$\partial_{11} u_1^+ = \frac{1}{k_f} \left[\frac{4\mu}{t} \left(\sum_{k=0,2}^p \gamma_k u_1^k \right) + \frac{8\mu}{t} \gamma^+ u_1^+ + \mu \Phi \partial_1 \Omega \right] \quad (21)$$

where "in-plane stiffness of the reinforcement" k_f , i.e., $N_{11}/\partial_1 u_1^+$, is defined as

$$k_f = \frac{E_f t_f}{1 - \nu_f^2} \quad (22)$$

with E_f and ν_f being respectively elasticity modulus and Poisson's ratio of the reinforcing sheet. The necessary boundary conditions for the solution of the governing equations, i.e., Eqs. (18) and (21), are the traction free boundary conditions (i.e., $\tau_{11}^n = 0$, $\tau_{12}^n = 0$) at the lateral bulge-free surfaces of the layer and the force-free boundary conditions (i.e., $N_{11} = 0$, thus, $\partial_1 u_1^+ = 0$) at the edges of the reinforcing sheets.

2.3 Solution of the warping problem using first order theory

To simplify the analysis of the layer under combined loading, it is desirable to make pure compressional, pure bending and pure warping deformations uncoupled from each other (Kelly 1994). Since the compressional deformation is already uncoupled from bending and warping deformations, to achieve such an uncoupling, it is sufficient to choose the warping shape so that the resultant axial force P and bending moment M associated with this warping deformation are zero. As proposed by Kelly (1994), selecting a cubic function, which can be written as

$$\Omega(x_1) = \left(\frac{x_1}{w} \right)^3 + f \left(\frac{x_1}{w} \right) \quad (23)$$

assures the first condition, i.e., the condition that P is zero. The constant f in Eq. (23), which is kept as an unknown warping-related constant until the analytical expressions are obtained for stress distributions, can, then, be computed from the condition that M has to be zero.

When the first order theory ($m=1$, $p=0$, $p'=1$, $\gamma_0=-3$, $\gamma_1=-15$, $\gamma^+=3/2$, $\gamma^-=3$ and $c_{10}=1$ with all other $c_{nj}=0$) is applied to the warping problem, one has, in view of Eqs. (15)-(16), three unknown displacements: two weighted

displacements, u_1^0 and u_2^1 , and one face displacement, u_1^+ . From these unknowns, u_1^0 and u_1^+ can be solved independently from u_2^1 . Coupled differential equations for u_1^0 and u_1^+ are obtained from Eq. (18) with $n=0$ and Eq. (21) using the relation given in Eq. (20). In view of Eq. (23), these equations are

$$\partial_{11}u_1^0 - \beta_{10}^2 [u_1^0 - u_1^+] = -\frac{\lambda + \mu}{\alpha} \frac{\Phi}{t} \left(\frac{3x_1^2}{w^3} + \frac{f}{w} \right) \quad (24)$$

with $\beta_{10}^2 = \frac{12\mu}{\alpha t^2}$

$$\partial_{11}u_1^+ - \beta_{11}^2 [u_1^+ - u_1^0] = \frac{\beta_{11}^2}{\beta_{10}^2} \frac{\mu}{\alpha} \frac{\Phi}{t} \left(\frac{3x_1^2}{w^3} + \frac{f}{w} \right) \quad (25)$$

with $\beta_{11}^2 = \frac{12\mu}{k_f t}$

One can see that Eqs. (24) and (25) are identical to Eqs. (74) and (75) in Pinarbasi and Mengi (2008). Thus, increasing the order of the theory from zero to one does not alter the form of the lateral displacements, i.e., u_1^0 and u_1^+ still have the following forms

$$u_1^0 = \left\{ \begin{array}{l} a_{11} \cosh(\beta_{10} x_1) + a_{11} \frac{\beta_{11}^2}{\beta_{10}^2} \frac{\lambda}{\beta_{11}^2} \frac{\Phi}{\alpha} \frac{1}{t} \left[\frac{x_1^4}{4w^3} + \frac{fx_1^2}{2w} \right] \\ + \frac{1}{\beta_{11}^2} \frac{\mu}{\alpha} \frac{\Phi}{t} \left[1 + \frac{\beta_{10}^2}{\beta_{11}^2} \frac{\lambda}{\mu} \left[\frac{3x_1^2}{w^3} \right] + \frac{1}{\beta_{10}^2} \frac{\mu}{\alpha} \frac{\Phi}{t} \left[1 + \frac{\beta_{10}^2}{\beta_{11}^2} \frac{\lambda}{\mu} \left[\frac{f}{w} + \frac{6}{w(\beta_{10} w)^2} \right] \right] \right] \end{array} \right\} \quad (26)$$

$$u_1^+ = \left\{ \begin{array}{l} -a_{11} \frac{\beta_{11}^2}{\beta_{10}^2} \cosh(\beta_{10} x_1) + a_{11} \frac{\beta_{11}^2}{\beta_{10}^2} \frac{\lambda}{\beta_{11}^2} \frac{\Phi}{\alpha} \frac{1}{t} \left[\frac{x_1^4}{4w^3} + \frac{fx_1^2}{2w} \right] \\ - \frac{\beta_{11}^2}{\beta_{10}^2} \frac{\mu}{\alpha} \frac{\Phi}{t} \left[1 + \frac{\beta_{10}^2}{\beta_{11}^2} \frac{\lambda}{\mu} \left[\frac{3x_1^2}{w^3} \right] \right] \end{array} \right\}$$

where

$$a_{11} = -\frac{\beta_{11}^2}{\beta_{10}^2} \frac{\Phi}{t} \frac{\lambda}{\alpha} \frac{1}{\beta_{10} \sinh(\beta_{10} w)} \left[1 + f + \frac{6}{(\beta_{10} w)^2} \left(1 + \frac{\mu}{\lambda} \frac{\beta_{11}^2}{\beta_{10}^2} \right) \right] \quad (27)$$

and $\beta_{11}^2 = \beta_{10}^2 + \beta_{11}^2$

The main effect of increasing the order of the theory is, in fact, to improve the axial displacement through the appearance of the weighted displacement u_2^1 in the governing equations. The equation associated with this new variable comes from Eq. (18) with $n=1$, which can be written in view of Eqs. (19)-(20), as

$$\partial_{11}u_2^1 - \beta_{21}^2 u_2^1 = \frac{2(\lambda + \mu)}{t} \frac{\Phi}{\mu} [\partial_1 u_1^0 - \partial_1 u_1^+] - \frac{10\alpha}{\mu t^2} \Phi \Omega \quad (28)$$

where $\beta_{21}^2 = \frac{60\alpha}{\mu t^2}$

From Eq. (26), one has

$$[\partial_1 u_1^0 - \partial_1 u_1^+] = a_{11} \frac{\beta_{11}^3}{\beta_{10}^2} \sinh(\beta_{10} x_1) \quad (29)$$

$$+ \frac{1}{\beta_{10}^2} \frac{\mu}{\alpha} \frac{\Phi}{t} \left[1 + \frac{\beta_{10}^2}{\beta_{11}^2} \frac{\lambda}{\mu} \right] \left[\frac{6x_1}{w^3} \right]$$

Thus, in view of Eq. (23), Eq. (28) becomes

$$\partial_{11}u_2^1 - \beta_{21}^2 u_2^1 = \left\{ \begin{array}{l} \frac{2(\lambda + \mu)}{t\mu} \left[a_{11} \frac{\beta_{11}^3}{\beta_{10}^2} \sinh(\beta_{10} x_1) \right. \\ \left. - \frac{10\alpha}{t} \frac{\Phi}{\mu} \frac{1}{t} \left(\frac{x_1^3}{w^3} + \frac{fx_1}{w} \right) \right. \\ \left. + \frac{1}{\beta_{10}^2} \frac{\mu}{\alpha} \frac{\Phi}{t} \left(1 + \frac{\beta_{10}^2}{\beta_{11}^2} \frac{\lambda}{\mu} \right) \left(\frac{6x_1}{w^3} \right) \right] \end{array} \right\} \quad (30)$$

It is clear that u_2^1 has the following form

$$u_2^1 = a_{22} \sinh(\beta_{21} x_1) + A \sinh(\beta_{10} x_1) + B x_1^3 + C x_1 \quad (31)$$

where the constants A , B and C (coming from the particular solution) are

$$A = \frac{2(\mu + \lambda)}{\mu t} \frac{\beta_{11}^3}{\beta_{10}^2} \frac{a_{11}}{\beta_{11}^2 - \beta_{21}^2}, \quad B = \frac{1}{\beta_{21}^2} \frac{10\alpha}{\mu} \frac{\Phi}{t} \frac{1}{w^3}, \quad (32)$$

$$C = \frac{6B}{\beta_{21}^2} - \frac{12}{\beta_{21}^2 \beta_{10}^2} \frac{\mu + \lambda}{\mu} \frac{\mu}{\alpha} \frac{\Phi}{t} \left[1 + \frac{\lambda}{\mu} \frac{\beta_{10}^2}{\beta_{11}^2} \right] \frac{1}{w^3} + \frac{1}{\beta_{21}^2} \frac{10\alpha}{\mu} \frac{\Phi}{t} \frac{f}{w}$$

and the constant a_{22} can be obtained from the boundary condition that $\tau_{12}^1|_{x_1=\pm w} = 0$, which yields

$$a_{22} = \frac{1}{\beta_{21} \cosh(\beta_{21} w)} \left\{ \begin{array}{l} \left[a_{11} \frac{2}{t} \frac{\beta_{11}^2}{\beta_{10}^2} - A \beta_{11} \right] \cosh(\beta_{10} w) - 3Bw^2 - C \\ + \frac{2}{\beta_{10}^2} \frac{\mu}{\alpha} \frac{\Phi}{t} \left[1 + \frac{\lambda}{\mu} \frac{\beta_{10}^2}{\beta_{11}^2} \right] \left[\frac{3+f}{w} + \frac{6}{w(\beta_{10} w)^2} \right] \end{array} \right\} \quad (33)$$

Once the governing equations are solved for the unknown displacements; i.e., for u_1^0 , u_2^1 and u_1^+ , the determination of displacement/stress distributions or any other parameter, such as, effective warping modulus of the layer, is straightforward (Pinarbasi and Mengi 2008). For FOT ($m=1$), the displacement distributions u_i ($i=1-2$) may be computed, in terms of u_i^n and S_i^\pm , from

$$u_i = u_i^0 + (3u_i^1) \left(\frac{2x_2}{t} \right) + \left(\frac{S_i^+}{2} - u_i^0 \right) \left(\frac{6x_2^2}{t^2} - \frac{1}{2} \right) \quad (34)$$

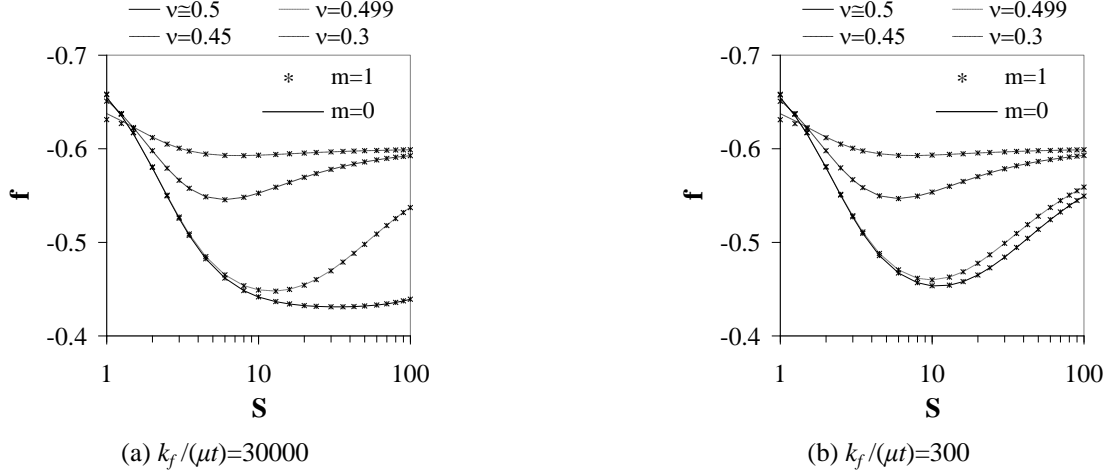
$$+ \left(\frac{S_i^-}{2} - 3u_i^1 \right) \left(\frac{20x_2^3}{t^3} - \frac{3x_2}{t} \right)$$

which, in view of Eq. (17), leads to

$$u_1 = \frac{3}{2} \left\{ a_{11} \frac{\beta_{11}^2}{\beta_{10}^2} \cosh(\beta_{10} x_1) + \frac{1}{\beta_{10}^2} \frac{\mu}{\alpha} \frac{\Phi}{t} \right. \quad (35)$$

$$\left. \left[1 + \frac{\lambda}{\mu} \frac{\beta_{10}^2}{\beta_{11}^2} \right] \left[\frac{3x_1^2}{w^3} + \frac{f}{w} + \frac{6}{w(\beta_{10} w)^2} \right] \right\} \left(1 - \frac{4x_2^2}{t^2} \right) + u_1^+$$

$$u_2 = \left\{ \begin{array}{l} 15 \left[a_{22} \sinh(\beta_{21} x_1) + A \sinh(\beta_{10} x_1) \right. \\ \left. + \Phi \left[\frac{x_1^3}{w^3} + f \frac{x_1}{w} \right] \left[\frac{10x_2^3}{t^3} - \frac{3x_2}{2t} \right] \right\}$$


 Fig. 3 Predictions of zeroth ($m=0$) and first ($m=1$) order theories for warping constant f

$$+ Bx_1^3 + Cx_1 \left[\frac{x_2}{t} - \frac{4x_2^3}{t^3} \right] \quad (35)$$

When Eq. (35) is compared with Eq. (83) in Pinarbasi and Mengi (2008), it may be seen that increasing the order of the theory from zero to one eliminates the commonly used assumption that the variation of axial displacement through the thickness is linear, resulting in advanced solutions for the axial displacement distribution and, in turn, for the stress distributions. These solutions are also free from the widely used incompressibility assumption for the material, inextensibility assumption for the sheets and the "pressure" assumption for the stress distributions in the layer.

Knowing the expressions for the displacement distributions, the expressions for the stress distributions can be obtained from linear theory. Then, the warping constant f appearing in Eq. (23) can be determined from the condition $M = \iint_A (\tau_{22}^\pm x_1) dA = 0$, where τ_{22}^\pm , i.e., axial face stresses, can be obtained, referring to Pinarbasi and Mengi (2008), from

$$\tau_{22}^\pm = \lambda \partial_1 u_1^\pm - \frac{30\alpha}{t} u_2^\pm + \frac{6\alpha}{t} \Phi \Omega(x_1) \quad (36)$$

The "effective warping modulus" E_w of the layer can be determined from

$$E_w = \frac{Q/(\Phi/t)}{J} \quad \text{with} \quad J = \int_A \Omega^2 dA \quad \text{and} \quad (37)$$

$$Q = \iint_A (\tau_{22}^\pm \Omega) dA$$

where Q is the resultant warping moment and J is the "warping" inertia.

Considering the complexity of the axial face stress expression and recalling that the determination of f requires the solution of an integral equation, it seems impractical to try to derive closed-form expressions for the predictions of FOT for f , so for E_w . Surely, numerical results can easily be obtained, for both f and E_w , using a mathematical program.

It can be recalled that ZOT has yielded the following closed form expressions for f and E_w (Pinarbasi and Mengi 2008)

$$f = - \frac{\left[1 - \frac{\beta_1 w}{\tanh(\beta_1 w)} \right] \left[1 + \frac{6}{(\beta_1 w)^2} \left(1 + \frac{\mu}{\lambda} \frac{\beta_1^2}{\beta_{10}^2} \right) \right] + 2 \left(1 + \frac{\mu}{\lambda} \frac{\beta_1^2}{\beta_{10}^2} \right) - \frac{(\beta_1 w)^2 \beta_{11}^2}{5 \beta_{10}^2} \left(1 - \frac{\beta_1^2 \alpha^2}{\beta_{11}^2 \lambda^2} \right)}{\left\{ \left[1 - \frac{\beta_1 w}{\tanh(\beta_1 w)} \right] - \frac{(\beta_1 w)^2 \beta_{11}^2}{3 \beta_{10}^2} \left(1 - \frac{\beta_1^2 \alpha^2}{\beta_{11}^2 \lambda^2} \right) \right\}} \quad (38)$$

$$E_w = \frac{\frac{\lambda^2 \beta_{10}^2}{\alpha \beta_{11}^2} \frac{1}{(\beta_1 w)^2} \left\{ \left(\frac{\alpha^2 \beta_{11}^2}{\lambda^2 \beta_{10}^2} - \frac{\beta_{11}^2}{\beta_{10}^2} \right) (\beta_1 w)^2 \left(\frac{1}{7} + \frac{2f}{5} + \frac{f^2}{3} \right) + \left(1 + \frac{\mu}{\lambda} \frac{\beta_1^2}{\beta_{10}^2} \right) \left(\frac{6}{5} + 2f \right) + \left(\frac{1}{7} + \frac{2f}{5} + \frac{f^2}{3} \right) \left[\left(1 + f + \frac{6}{(\beta_1 w)^2} \right) \left(1 - \frac{\beta_1 w}{\tanh(\beta_1 w)} \right) + 2 \right] \left[1 + f + \frac{6}{(\beta_1 w)^2} \left(1 + \frac{\mu}{\lambda} \frac{\beta_1^2}{\beta_{10}^2} \right) \right] \right\}}{\left(\frac{1}{7} + \frac{2f}{5} + \frac{f^2}{3} \right)} \quad (39)$$

Inextensible reinforcement case (i.e., $k_f \rightarrow \infty$ which means that $u_1^+ = 0$) may have particular concern. For this special case, the predictions of ZOT for f and E_w , denoted as f_{inex} and $E_{w,inex}$, are

$$f_{inex} = - \frac{\left[1 - \frac{\beta_{10} w}{\tanh(\beta_{10} w)} \right] \left[1 + \frac{6}{(\beta_{10} w)^2} \left(1 + \frac{\mu}{\lambda} \right) \right] + 2 \left(1 + \frac{\mu}{\lambda} \right) - \frac{(\beta_{10} w)^2}{5}}{\left\{ \left[1 - \frac{\beta_{10} w}{\tanh(\beta_{10} w)} \right] - \frac{(\beta_{10} w)^2 \alpha^2}{3 \lambda^2} \right\}} \quad (40)$$

$$E_{w,inex} = \frac{\frac{\lambda^2}{\alpha} \frac{1}{(\beta_{10} w)^2} \left\{ \left(\frac{\alpha^2}{\lambda^2} (\beta_{10} w)^2 \left(\frac{1}{7} + \frac{2f}{5} + \frac{f^2}{3} \right) + \left(1 + \frac{\mu}{\lambda} \right) \left(\frac{6}{5} + 2f \right) + \left(\frac{1}{7} + \frac{2f}{5} + \frac{f^2}{3} \right) \left[\left(1 + f + \frac{6}{(\beta_{10} w)^2} \right) \left(1 - \frac{\beta_{10} w}{\tanh(\beta_{10} w)} \right) + 2 \right] \left[1 + f + \frac{6}{(\beta_{10} w)^2} \left(1 + \frac{\mu}{\lambda} \right) \right] \right\}}{\left(\frac{1}{7} + \frac{2f}{5} + \frac{f^2}{3} \right)} \quad (41)$$

3. Behavior of strip-shaped fiber-reinforced elastomeric isolators under pure warping

For a fiber-reinforced elastomeric isolator subjected to pure warping, there are two limiting cases with regard to the stiffness (k_f) of the reinforcing sheets: (i) completely extensible reinforcement case, which occurs when $k_f \rightarrow 0$, and (ii) completely inextensible reinforcement case, which occurs when $k_f \rightarrow \infty$. In this section, warping behavior of

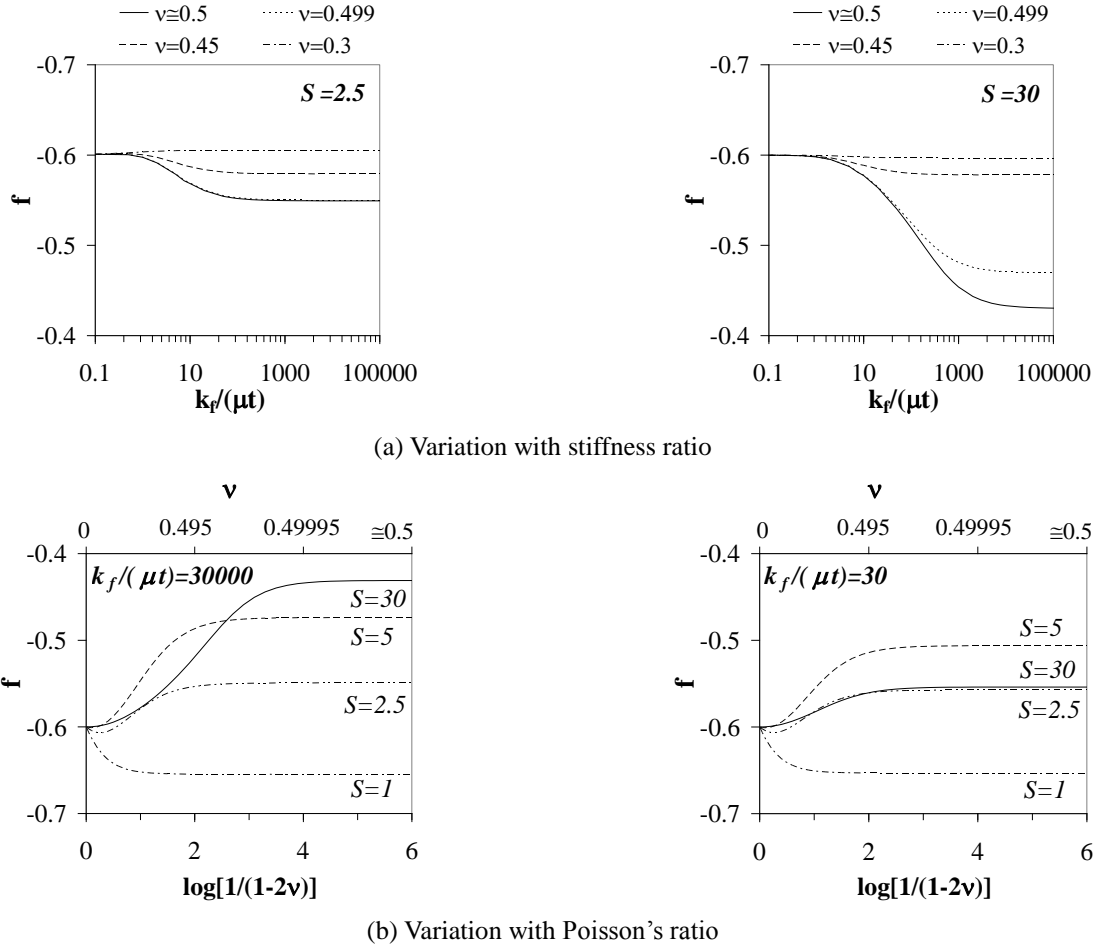


Fig. 4 Variations of warping constant f with stiffness ratio and Poisson's ratio

fiber-reinforced isolators is studied in detail by using the analytical solutions derived in the previous section. Particular emphasis is given to the investigation of the effects of three key parameters; namely, $k_f^* = k_f / \mu t$ (stiffness ratio for the individual bonded elastomer layer, i.e., stiffness of the reinforcing sheets with respect to that of the layer), S (shape factor of the isolator, i.e., the ratio of one loaded area of the bonded elastomer layer to its free-to-bulge areas) and ν (Poisson's ratio of the elastomer), on warping constant f , warping modulus E_w and stress distributions in the isolator.

3.1 Warping constant

Warping behavior of a fiber-reinforced elastomeric isolator is mainly controlled by the warping pattern of the reinforcements, thus by the warping constant " f ". As already mentioned, even though it is impractical to derive a closed-form expression for f when FOT is used in the formulation due to the highly nonlinear stress expressions, it is possible to compute f numerically and compare the numerical results with the predictions of ZOT computed from Eq. (38).

Fig. 3 compares the predictions of ZOT and FOT for f for two different stiffness ratios, $k_f^* = 30000$ and 300 , and various shape factors and Poisson's ratios. It is to be noted that the shape factor of a strip-shaped layer with a thickness

t and width $2w$ equals to $S = w/t$. As shown in the graphs, the predictions of both theories are almost identical in the studied ranges of parameters. Thus, Eq. (38) can be used to calculate f even when the FOT is used in the analytical formulation.

It can be inferred from Kelly (1994) that there are two limiting values for f : $f_u = -3/5 = -0.6$, which is the value obtained for an unbonded uniform short "beam", and $f_b = -3/7 \approx -0.43$, which is the value predicted by the "pressure method" (PM) for an "incompressible" strip-shaped isolator reinforced with "inextensible" sheets. Fig. 3(a) shows that, for $k_f^* = 30000$, the f values for high shape factor (HSF) isolators are equal to f_b when $\nu = 0.5$, indicating that HSF isolators behave as if they were reinforced with inextensible sheets when $k_f^* = 30000$. Calculated using $E_f = 210$ GPa, $\nu_f = 0.3$, $t_f = 0.27$ mm, $t = 3$ mm and $\mu = 0.7$ MPa, this value of k_f^* corresponds approximately to a typical value for the stiffness ratio of rubber-fiber reinforcement unit commonly used in seismic isolation bearings (Kelly 2002). From Fig. 3, it can also be seen that f values for HSF isolators become equal to f_u when Poisson's ratio is sufficiently low (e.g., when $\nu = 0.3$). This conclusion is valid even when the stiffness ratio is considerably large (see Fig. 3(a)).

However, it is not so easy to understand the effects of

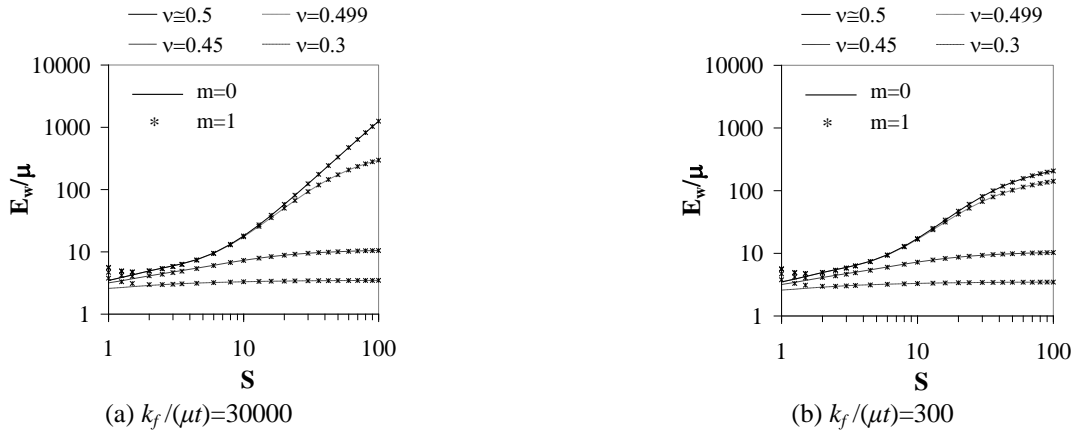


Fig. 5 Predictions of zeroth ($m=0$) and first ($m=1$) order theories for warping modulus E_w

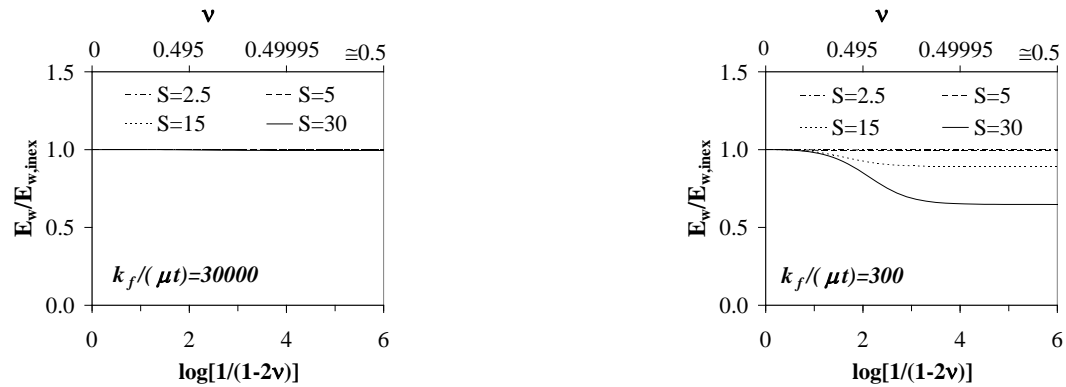
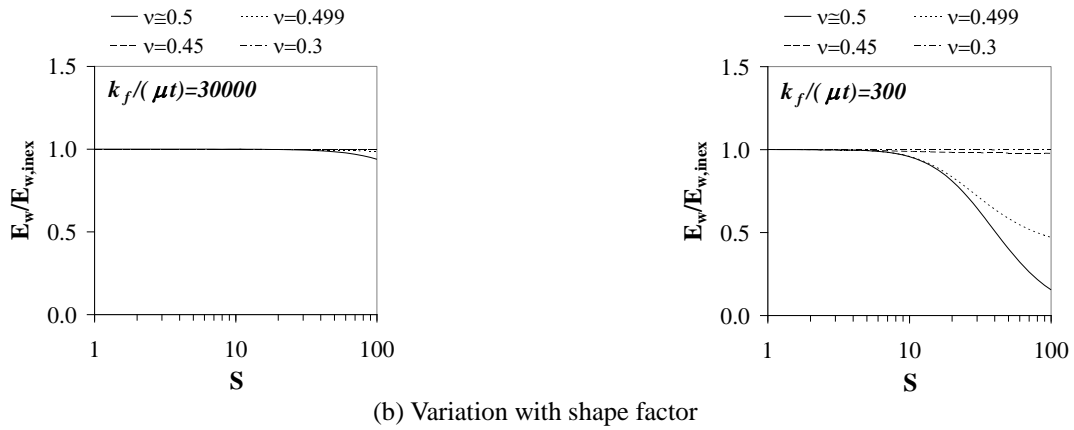
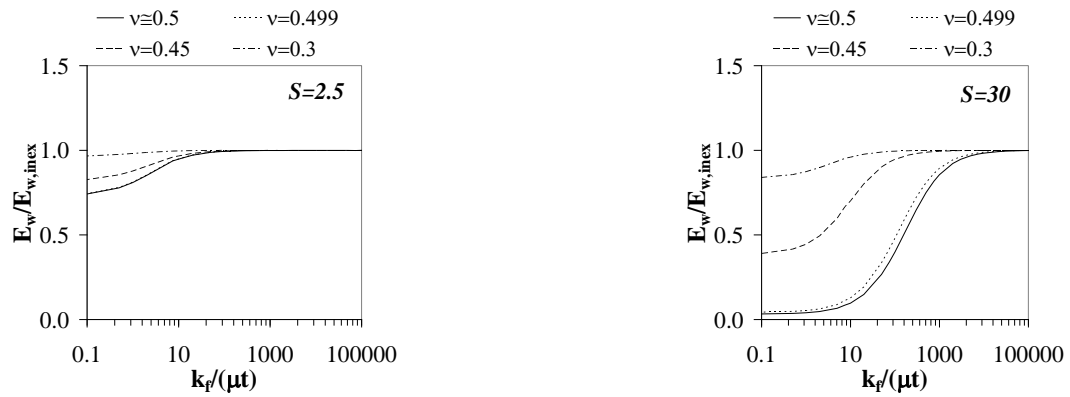


Fig. 6 Effect of reinforcement flexibility on normalized warping modulus

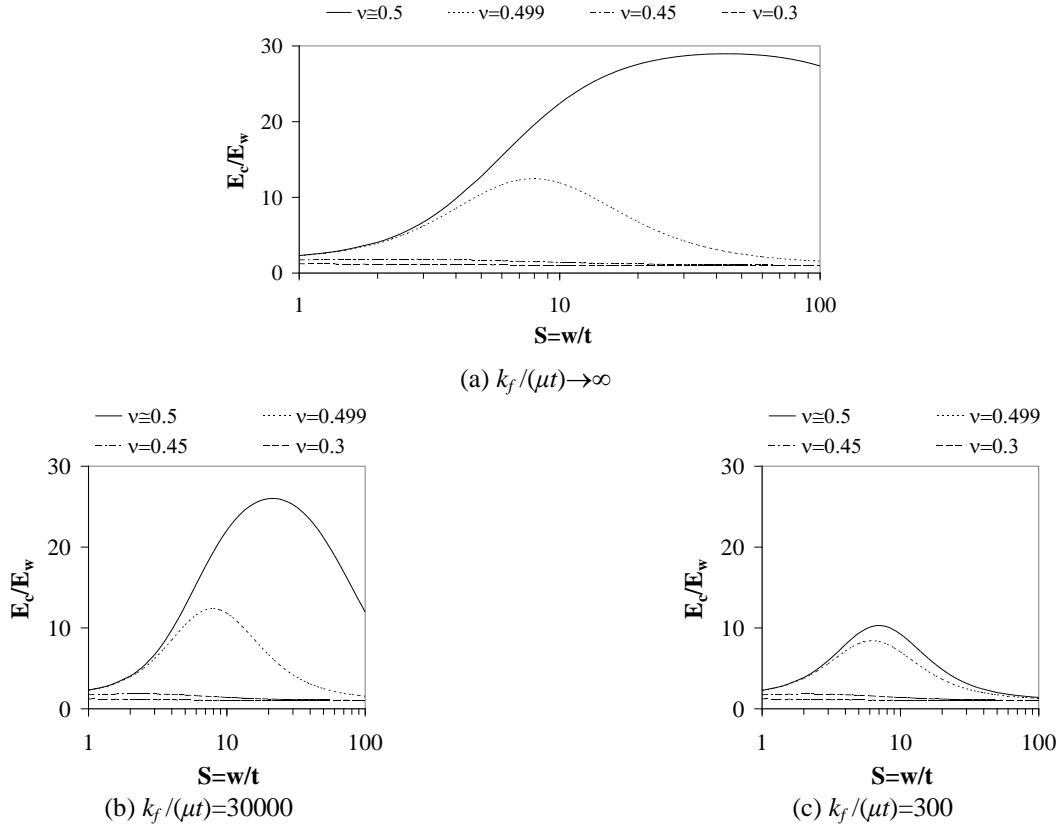


Fig. 7 Effect of reinforcement flexibility on E_c/E_w ratio

stiffness ratio and Poisson's ratio on warping constant for low shape factor (LSF) isolators from the plots presented in Fig. 3. For a thorough investigation on the effects of reinforcement flexibility and elastomer compressibility on f , the variations of f with k_f^* and ν are plotted and presented in Fig. 4. The graphs in Fig. 4 clearly show that f approaches f_u as $k_f^* \rightarrow 0$ and/or $\nu \rightarrow 0$. This conclusion is valid both for LSF and HSF isolators. A similar conclusion is partially valid for f_b ; f approaches to f_b when $k_f^* \rightarrow \infty$ and $\nu \rightarrow 0.5$ only if S is sufficiently large since the pressure method (PM) is valid only for HSF isolators.

3.2 Warping modulus

Fig. 5 compares the predictions of FOT and ZOT for warping modulus E_w for two different stiffness ratios and various shape factors and Poisson's ratios. It is seen that the predictions of both theories for E_w almost exactly match in the studied ranges of parameters. Thus, the closed-form expression in Eq. (39) can be used to compute E_w values when FOT is used in the formulation.

To investigate the effect of reinforcement flexibility on E_w in more detail, the variations of the normalized warping modulus with k_f^* , S and ν are plotted in Figs. 6(a)-(c). In these plots, E_w values are normalized by $E_{w,inex}$ values computed from Eq. (41). Fig. 6(a) shows that $E_w \rightarrow E_{w,inex}$ as $k_f^* \rightarrow \infty$.

While an HSF isolator attains its inextensible-reinforcement behavior at considerably large values of k_f^* ,

especially if ν is close to 0.5, there is no need to have very large values of k_f^* for an LSF isolator to behave as if it were bonded to inextensible reinforcements. From Figs. 6(b), (c), it is seen that 30000 is a sufficiently large value for the stiffness ratio, even for incompressible HSF isolators, to use $E_{w,inex}$ instead of E_w in the design of fiber-reinforced isolators. The effect of reinforcement flexibility has to be considered, however, for smaller stiffness ratios, e.g., $k_f^*=300$, especially if S is large and ν is close to 0.5. For LSF isolators of compressible materials, the inextensible-reinforcement assumption is valid even when $k_f^*=300$.

In the analysis of a multi-layered elastomeric isolator, it is a common practice to represent its bending or warping modulus, i.e., E_b or E_w , in terms of its compression modulus E_c (e.g., Kelly 1994). In Fig. 7, the E_c/E_w ratio is plotted for various S , ν and k_f^* values (for the calculation of E_c values, the third of Eq. (54) in Pinarbasi and Mengi (2008) is used). It is worth noting that the PM prediction for the E_c/E_w ratio is 30 for "incompressible" layers bonded to "inextensible" reinforcements (Kelly 1994). As shown in Fig. 7(a), FOT prediction for the E_c/E_w ratio also tends to 30 as $k_f^* \rightarrow \infty$ and $\nu \rightarrow 0.5$ provided that S is sufficiently large. However, as seen from Figs. 6(b), (c), this ratio can be much smaller than 30 especially if S , ν or k_f^* are small. Then, taking $E_c/E_w = 30$ may significantly underestimate the true value of the warping modulus.

3.3 Stress distributions

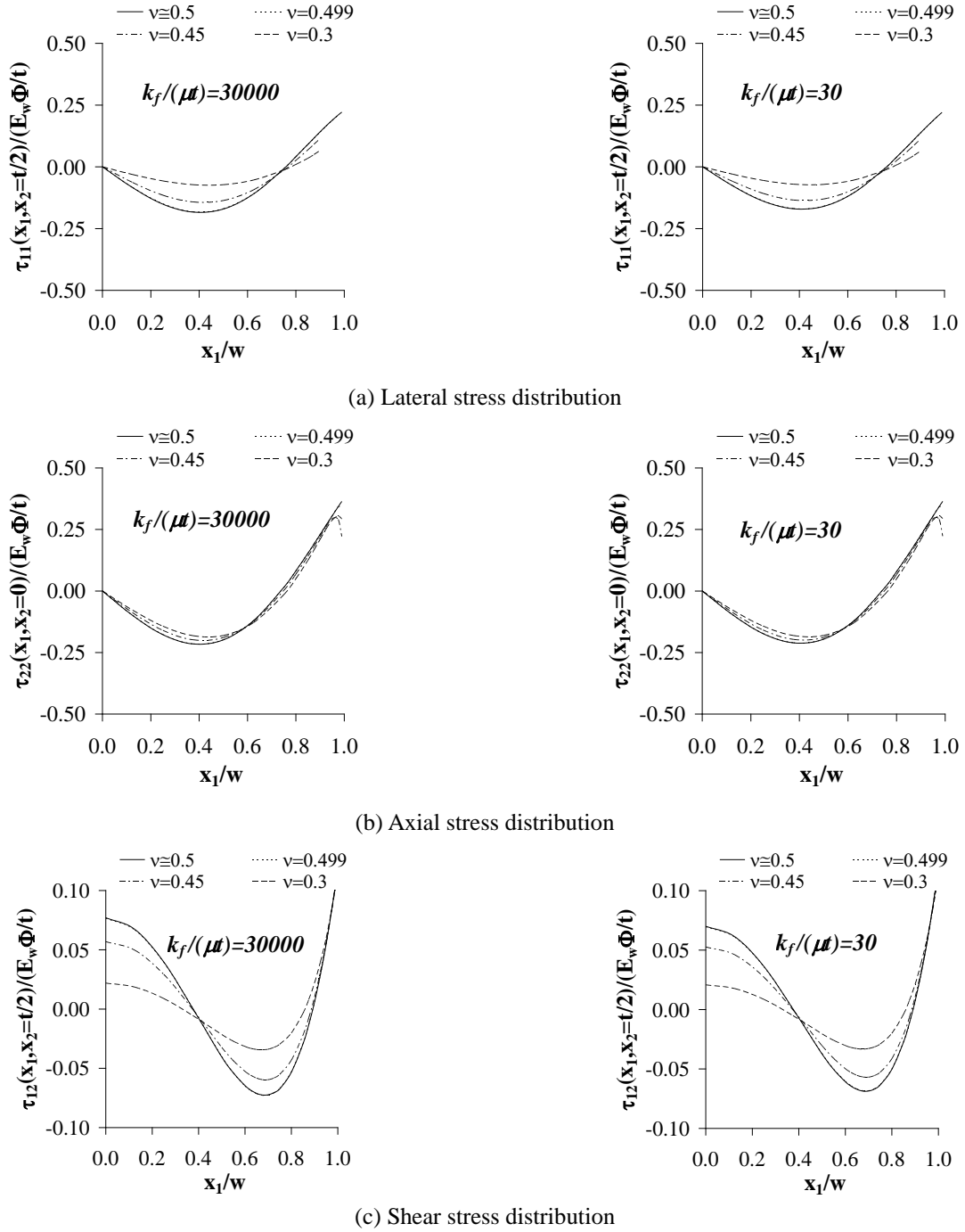


Fig. 8 Effect of reinforcement flexibility on stress distributions in lateral direction for $S=2.5$

The graphs presented in Figs. 8 to 10 show stress distributions, in lateral direction, for an interior elastomer layer in a strip-shaped fiber-reinforced elastomeric isolator under pure warping for various Poisson's ratios and two shape factors; $S=2.5$, representing LSF isolators, and $S=30$, representing HSF isolators. Since an LSF isolator is not influenced from reinforcement flexibility unless k_f^* is considerably low, the graphs in Fig. 8 are plotted only for two particular values of k_f^* ; 30000 and 30. On the other hand, the graphs in Figs. 9 and 10 are plotted for $k_f^*=30000, 3000, 300, 30$ to show the effect of reinforcement flexibility on warping behavior of an HSF isolator clearly. In the

graphs, stress distributions are plotted over their most critical sections (i.e., τ_{11} and τ_{12} at $x_2=\pm t/2$, and τ_{22} at $x_2=0$) and stress values are normalized by $E_w\Phi/t$. It can be noted that the axial stress in a uniform short beam under pure warping, which can be written in the notation of the present formulation as $\sigma_{22} = E\Omega(x_1)\partial_2\Phi(x_2)$ (refer to Kelly (1994) for details), reaches its maximum value, $(\sigma_{22})_{\max} = 0.4E\partial_2\Phi$, at the edges of the layer, i.e., at $x_1=\pm w$, if the cubic function in Eq. (23) is selected as the warping function. Thus, normalizing the stress values by $E_w\Phi/t$ can be considered as a kind of normalization by a factor of

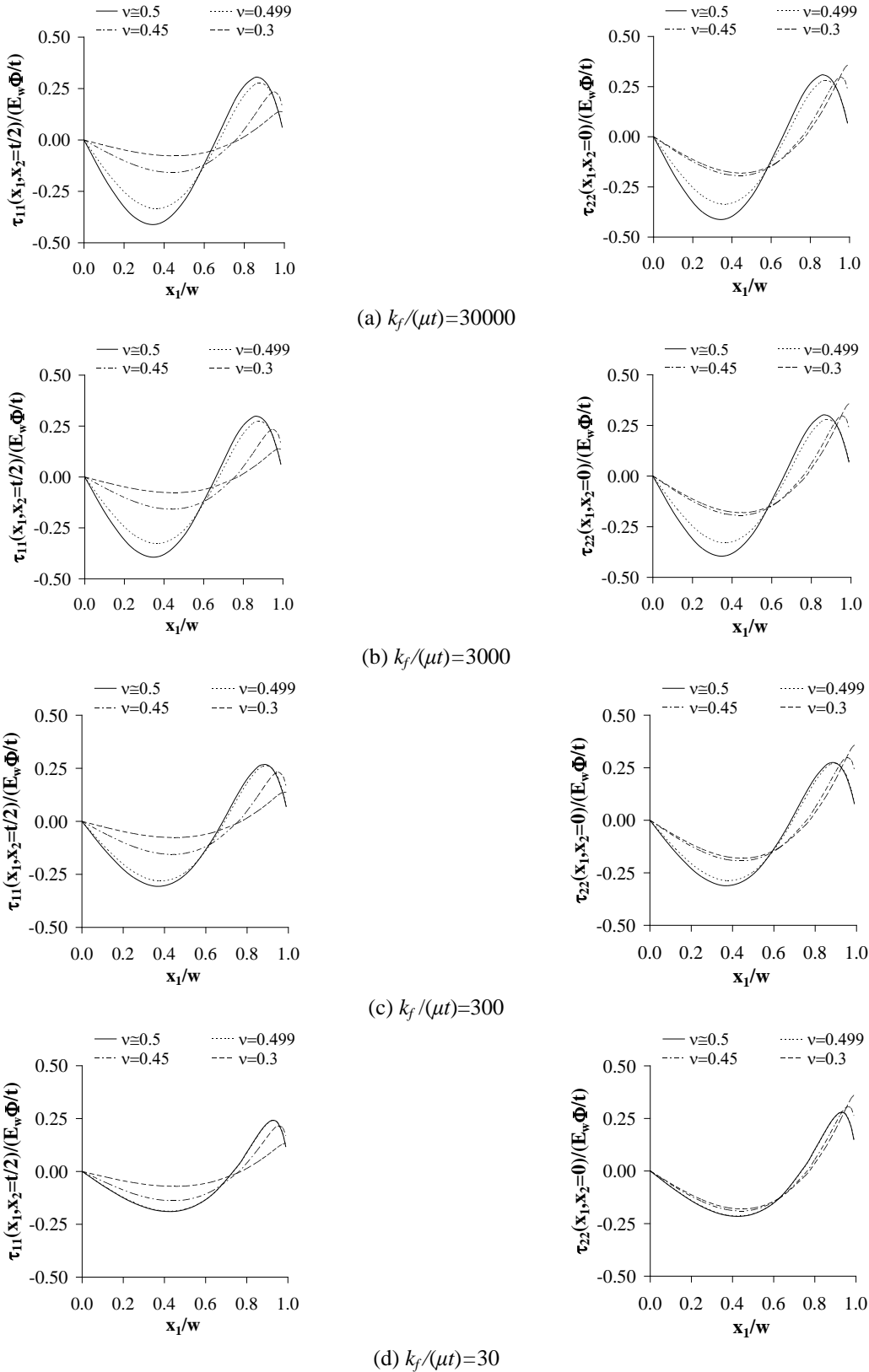
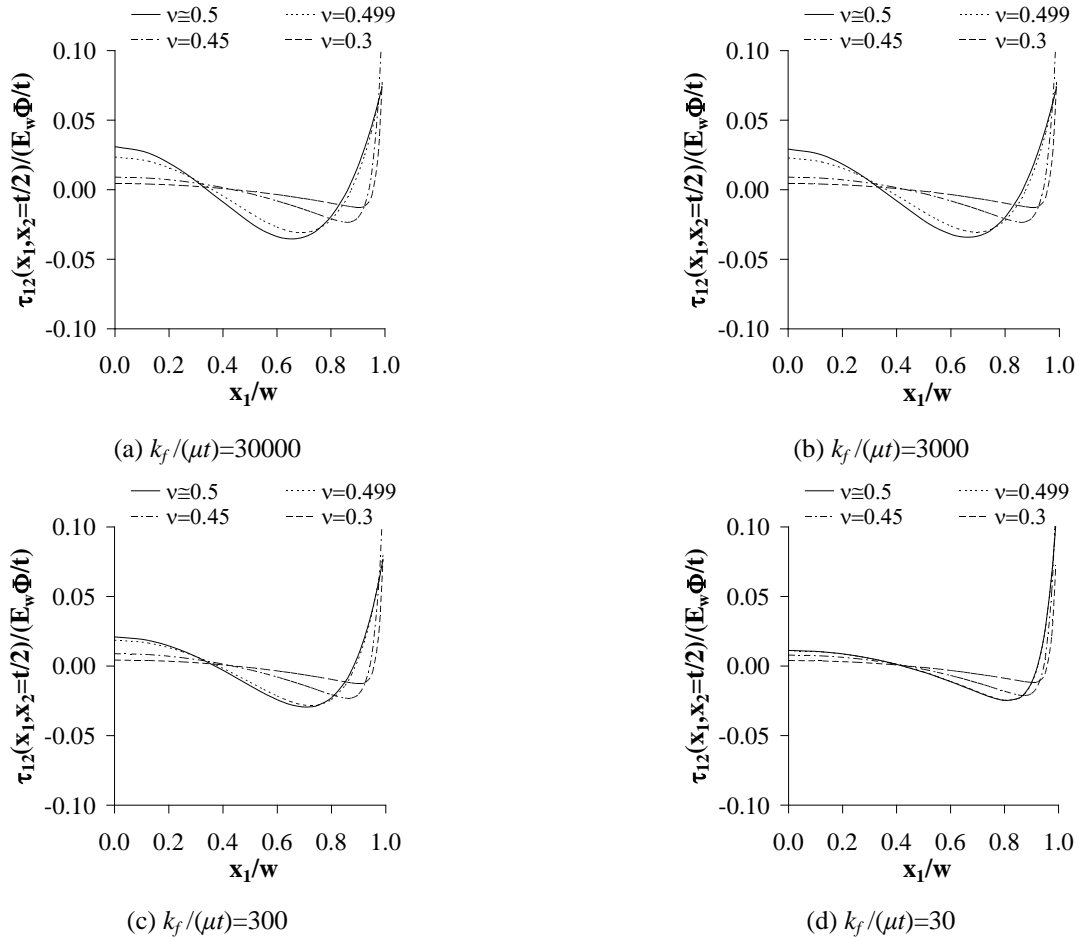
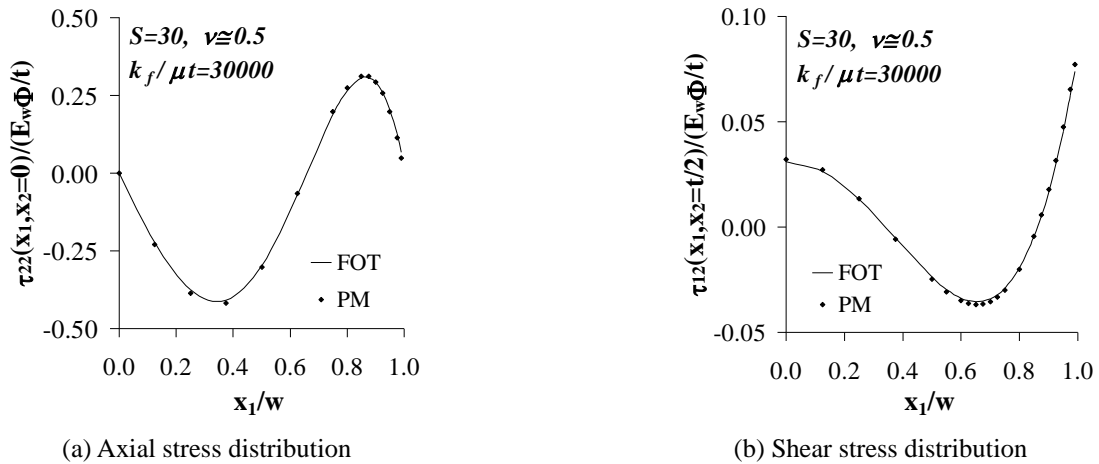


Fig. 9 Effect of reinforcement flexibility on normal stress distributions in lateral direction for $S=30$

maximum axial stress developing in the corresponding unreinforced isolator as predicted by the short beam theory.

From Fig. 8, it is seen that an LSF isolator ($S=2.5$) behaves as if it were bonded to inextensible reinforcements

even when $k_f^*=30$. This means that warping behavior of LSF isolators can satisfactorily be predicted by using the expressions derived based on inextensible-reinforcement assumption. Fig. 8 also shows that while axial stress


 Fig. 10 Effect of reinforcement flexibility on shear stress distribution in lateral direction for $S=30$

 Fig. 11 Convergence of FOT predictions to PM predictions for stress distributions in an “incompressible” HSF isolator ($S=30$) reinforced with nearly inextensible sheets

distribution is almost insensitive to the changes in Poisson’s ratio, lateral normal and shear stress decrease as ν decreases. It can also be concluded that warping behavior of an LSF isolator is not affected from the presence of slight compressibility: stress distributions for $\nu=0.495$ and $\nu=0.5$ coincide. This is mainly due to the fact that an LSF isolator reaches its incompressible behavior at a smaller value of ν

(see Fig. 3(b)).

Unlike an LSF isolator, the warping behavior of an HSF ($S=30$) isolator is influenced from the reinforcement flexibility, considerably (Fig. 9). In general, it can be said that k_f^* affects the stress distributions in the same way that ν does: the shapes of the normal stress distributions change approximately from a fifth degree polynomial to a third

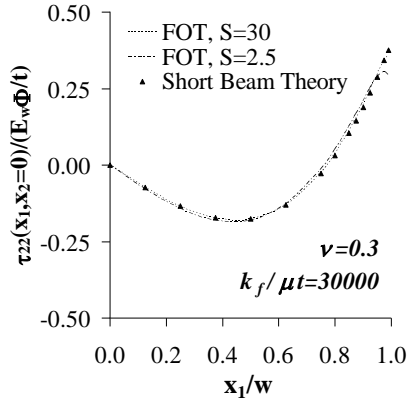


Fig. 12 Convergence of FOT solution to the “short beam” solution for axial stress distribution in compressible ($\nu=0.3$) LSF ($S=2.5$) and HSF ($S=30$) isolators reinforced with nearly inextensible sheets

degree polynomial and the normal stress values decrease as k_f^* or ν decreases until the completely-flexible-reinforcement behavior is reached. As far as the shear stress distributions are concerned (Fig. 10), the effect of ν on the behavior is significant especially if k_f^* is large. The main effect of decreasing k_f^* or ν on shear stress is to decrease stress values in the layer, except at the edges. If Fig. 10 is compared with Fig. 8(c), it can be seen that for the same values of k_f^* and ν , the normalized shear stress in an LSF isolator is, in general, larger than that in an HSF isolator.

Figs. 9-10 also shows that the warping behavior of an HSF isolator can be influenced from the presence of slight compressibility ($\nu=0.495$) significantly: stress distributions for $\nu=0.495$ deviate from those for $\nu=0.5$ considerably if k_f^* is large. This shows the significance of including the material compressibility in analysis of HSF isolators reinforced with nearly/completely inextensible sheets. It is also to be noted that the difference in warping behavior of HSF isolators of strictly and nearly incompressible materials disappears as k_f^* decreases. In the limit, when k_f^* is sufficiently small (e.g., when $k_f^*=30$), stress distributions for $\nu=0.495$ and $\nu=0.5$ overlap. This is due to the fact that an HSF isolator with a smaller k_f^* reaches its incompressible behavior at a smaller value of ν than a layer with the same S , but, with a larger k_f^* (also see Fig. 4(b)).

As expected, FOT solutions converge to “incompressible and inextensible” PM solutions when $\nu \rightarrow 0.5$, $k_f^* \rightarrow \infty$ and S is large. This can be seen from Fig. 11, where the predictions of FOT and PM for axial and shear stress distributions in lateral direction in an isolator with $S=30$ are compared for $k_f^*=30000$. The “incompressible and inextensible” PM expressions Kelly (1994) for the normalized axial and shear stresses can be expressed, in the notation of the formulation, in the following forms

$$\frac{\tau_{22,PM}}{E_w \Phi/t} = -\frac{9}{2} \left(\frac{x_1^5}{w^5} - \frac{10}{7} \frac{x_1^3}{w^3} + \frac{3}{7} \frac{x_1}{w} \right) \quad (42)$$

$$\frac{\tau_{12,PM}}{E_w \Phi/t} = \frac{9}{4S} \left(5 \frac{x_1^4}{w^4} - \frac{30}{7} \frac{x_1^2}{w^2} + \frac{3}{7} \right)$$

On the other hand, for compressible materials, the axial stress distribution in an HSF isolator is much closer to the predictions of the short beam theory. For $\nu=0.3$, the predictions of both theories are almost identical even for an LSF isolator, as shown in Fig. 12. It is to be noted that the prediction of the short beam theory for the normalized axial stress simply equals to the warping shape. Fig. 12 also shows that an HSF isolator of highly compressible material behaves as if it were an unreinforced isolator even when $k_f^*=30000$.

The plots in Figs. 8-10 also provide information about the locations and magnitudes of maximum stresses developing in a fiber-reinforced elastomeric isolator under pure warping. From Figs. 8 and 9, one can notice that the normal stress distributions have two extreme points in the range $0 \leq x_1/w \leq 1.0$. Eq. (42) indicates that for axial stress distribution in an HSF isolator of incompressible materials and inextensible reinforcements, these critical points occur at $x_1 \cong 0.34w$ and $x_1 \cong 0.86w$, with corresponding peak values -0.42 and 0.31 , respectively. It is interesting to see that the normalized peak values do not depend on the geometric properties of the individual elastomer layer. Since warping behavior of an isolator tend to short beam behavior as reinforcement extensibility or material compressibility increases, these critical points move toward $x_1 \cong 0.45w$ and $x_1=w$, which are the two extreme points for the cubic warping shape when $f=-3/5$, as k_f^* or ν decreases. The peak values also change to -0.18 at $x_1 \cong 0.45w$ and to 0.4 at $x_1=w$.

Similarly, from Figs. 8(c) and 10, it is seen that, as far as the shear stress distributions are concerned, there are three critical points in the range $0 \leq x_1/w \leq 1$. Two of them have fixed locations: at the center of the layer ($x_1=0$) and at the edge ($x_1=w$). PM predicts the location of the third critical point as $x_1 = \sqrt{3/7} w$ for HSF isolators with incompressible materials and inextensible reinforcements, and the peak values for the normalized shear stress as approximately $\{0.96/S, -1.10/S, 2.57/S\}$ at respectively $x_1 = \{0, \sqrt{3/7} w, w\}$. When k_f^* or ν decreases, the location of the critical point near the center of the half-width moves towards the edge and the normalized shear stress over the cross section reduces, except at the edges. At the limit, when an isolator starts to behave as if it were a short uniform beam, shear stress is concentrated only on the edges.

Using the advanced stress expressions derived from FOT, it is also possible to study the effect of reinforcement flexibility on stress distributions in axial direction. The graphs in Figs. 13 and 14 plot normal stress distributions at the vertical section $x_1=0.35w$ and shear stress distributions at $x_1=0.65w$, which are very close to the critical points discussed above for HSF isolators with incompressible materials and inextensible reinforcements, for two different shape factors; $S=2.5$ and $S=30$. The effect of reinforcement flexibility on stress distributions is examined by plotting the graphs for two specific values of stiffness ratio; $k_f^*=30000$ and 30 .

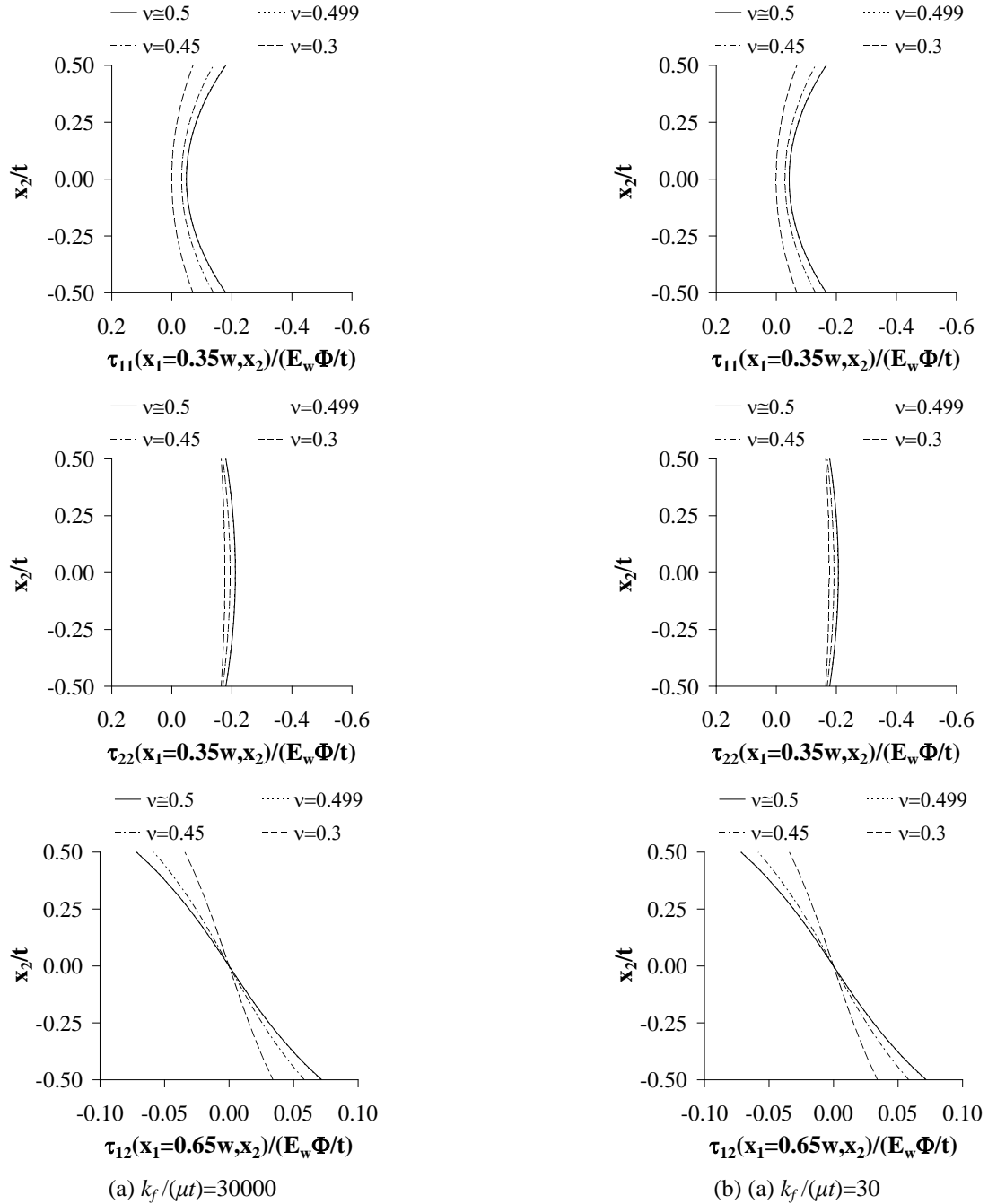


Fig. 13 Effect of reinforcement flexibility on stress distributions in axial direction under pure warping for $S=2.5$

Fig. 14 shows that normal stresses are uniformly and shear stress is linearly distributed through the individual layer thickness in an HSF isolator, which is not valid, in general, for LSF isolator, as shown in Fig. 13. It can also be seen that the pressure assumption is valid only for HSF isolators with nearly incompressible materials provided that the reinforcements are not too flexible. From the graphs plotted for $S=30$ and $k_f^*=30$, one can observe that the axial stress is no longer equal to the lateral normal stress at the studied section even when $\nu \approx 0.5$.

4. Conclusions

As pointed out by Kelly (1994), the buckling analysis of a multi-layered elastomeric isolator necessitates the analysis of an individual bonded elastomer layer not only under compressional and bending deformations but also under "warping" (distortional) deformations if the interior reinforcing sheets are extensible. This paper presents a detailed study on "warping" behavior of long rectangular elastic strips bonded to flexible reinforcements.

Main conclusions can be summarized as follows:

- The effect of reinforcement flexibility on warping behavior depends mainly on stiffness of the reinforcement (k_f), shape factor of the isolator (S) and Poisson's ratio of the elastomer (ν). For a typical fiber-

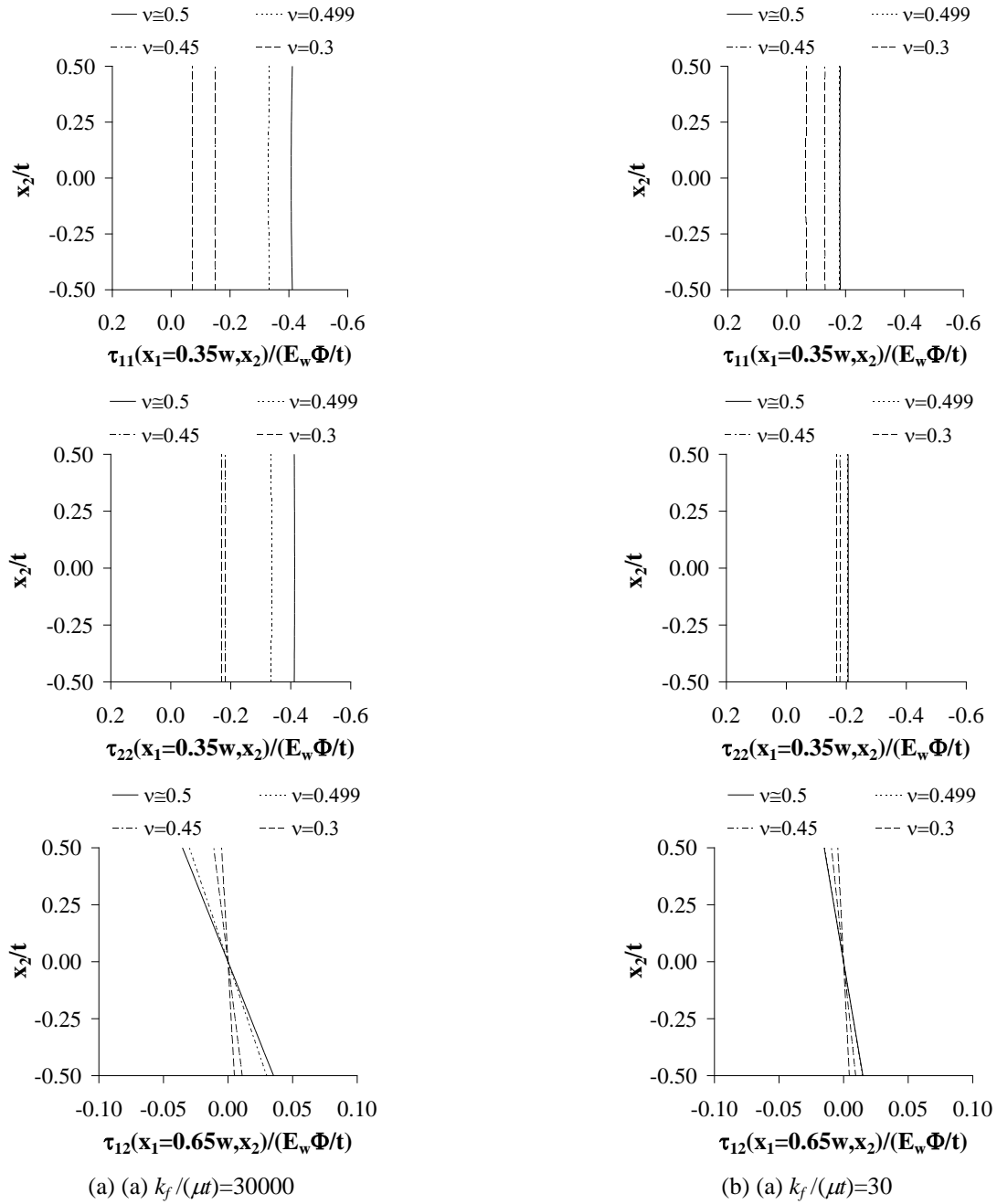


Fig. 14 Effect of reinforcement flexibility on stress distributions in axial direction under pure warping for $S=30$

reinforced elastomeric isolator used in *seismic isolation technique* ($E_f=210$ GPa, $\nu_f=0.3$, $t_f=0.27$ mm, $t=3$ mm and $\mu=0.7$ MPa, for which $k_f^*=k_f/\mu t \approx 30000$), the effect of reinforcement flexibility can be ignored and the effective warping modulus (E_w) can be computed from Eq. (41). However, the use of $f_b=-3/7$ in the calculation of E_w is not suggested even when S is large since the presence of even slight compressibility (e.g., $\nu=0.495$) can change f significantly.

• The widely used pressure method (PM) is valid only when S is large, $\nu=0.5$ and $k_f \rightarrow \infty$. The prediction of PM for the E_c/E_w ratio (where E_c is the compression modulus of the isolator), i.e., 30, may significantly underestimate the true value of E_w for isolators with low

shape factors and/or compressible materials and/or extensible reinforcement.

• There are two critical points in normal stress distributions along the lateral direction in the range $0 \leq x_1/w \leq 1.0$. These points are located at $x_1 \approx 0.34w$ and $x_1 \approx 0.86w$, with corresponding normalized peak values of -0.42 and 0.31 when S is large, $\nu=0.5$ and $k_f \rightarrow \infty$. As ν or k_f decreases, these critical points move towards $x_1 \approx 0.45w$ and $x_1=w$ with the normalized peak values -0.18 and 0.4 , respectively. As far as the shear stress distributions are concerned, there are three critical points in the same range. When S is large, $\nu=0.5$ and $k_f \rightarrow \infty$, these points are located at $x_1 = \{0, \sqrt{3/7} w, w\}$,

with corresponding normalized peak values of $\{0.96/S, -1.10/S, 2.57/S\}$. When k_f or ν decreases, the location of the critical point near the center of the half-width moves towards the edge and the shear stress over the cross section reduces, except at the edges.

Free from four commonly used assumptions in literature; (i) incompressibility assumption for the elastomer material, (ii) inextensibility assumption for the reinforcing sheets, (iii) “pressure” assumption for the stress distributions and (iv) the assumption that the axial displacement varies linearly through the layer thickness, the closed form expressions derived in the paper for warping behavior can effectively be used in buckling analysis of multi-layered fiber reinforced isolators/bearings even when the shape factor is small, elastomer material is compressible or reinforcing sheets are extensible.

References

- Angeli, P., Russo, G. and Paschini, A. (2013), “Carbon fiber-reinforced rectangular isolators with compressible elastomer: Analytical solution for compression and bending”, *Int. J. Solid. Struct.*, **50**(22-23), 3519-3527.
- Gent, A.N. and Lindley, P.B. (1959), “The compression of bonded rubber blocks”, *P. I. Mech. Eng.*, **173**(3), 111-122.
- Kelly, J.M. (1994), *The influence of Plate Flexibility on the Buckling Load of Elastomeric Isolators*, Report UCB/EERC-94/03, Earthquake Engineering Research Center, University of California, Berkeley, California, USA.
- Kelly, J.M. (1997), *Earthquake Resistant Design with Rubber*, Springer-Verlag, London.
- Kelly, J.M. (1999), “Analysis of fiber-reinforced elastomeric isolators”, *J. Seismol. Earthq. Eng.*, **2**(1), 19-34.
- Kelly, J.M. and Takhirov, S.M. (2001), *Analytical and Experimental Study of Fiber-Reinforced Elastomeric Isolators*, PEER Report 2001/11, Pacific Earthquake Engineering Research Center, University of California, Berkeley, California, USA.
- Kelly, J.M. (2002), “Seismic isolation systems for developing countries”, *Earthq. Spectra*, **18**(3), 385-406.
- Kelly, J.M. and Konstantinidis D. (2011), *Mechanics of Rubber Bearings for Seismic and Vibration Isolation*, John Wiley and Sons Ltd, UK.
- Kelly, J.M. and Calabrese, A. (2012). *Mechanics of Fiber Reinforced Bearings*, PEER Report 2012/101, Pacific Earthquake Engineering Research Center, University of California, Berkeley, California, USA.
- Mengi, Y. (1980), “A new approach for developing dynamic theories for structural elements Part 1: Application to thermoelastic plates”, *Int. J. Solid. Struct.*, **16**(12), 1155-1168.
- Osgooei, P.M., Tait, M.J. and Konstantinidis, D. (2014), “Three-dimensional finite element analysis of circular fiber-reinforced elastomeric bearings under compression”, *Compos. Struct.*, **108**, 191-204.
- Osgooei, P.M., Engelen, N.C.V., Konstantinidis, D. and Tait, M.J. (2015), “Experimental and finite element study on lateral response of modified rectangular fiber-reinforced elastomeric isolators (MR-FREIs)”, *Eng. Struct.*, **85**, 293-303.
- Pinarbasi, S., Akyuz, U. and Mengi, Y. (2006), “A new formulation for the analysis of elastic layers bonded to rigid surfaces”, *Int. J. Solid. Struct.*, **43**(14), 4271-4296.
- Pinarbasi, S. and Mengi, Y. (2008), “Elastic layers bonded to flexible reinforcements”, *Int. J. Solid. Struct.*, **45**(3), 794-820.
- Pinarbasi, S., Mengi, Y. and Akyuz, U. (2008), “Compression of solid and annular circular discs bonded to rigid surfaces”, *Int. J. Solid. Struct.*, **45**(16), 4543-4561.
- Pinarbasi, S. and Okay, F. (2011), “Compression of hollow-circular fiber-reinforced rubber bearings”, *Struct. Eng. Mech.*, **38**(3), 361-384.
- Toopchi-Nezhad, H., Tait, M.J. and Drysdale, R.G. (2011), “Bonded versus unbonded strip fiber reinforced elastomeric isolators: finite element analysis”, *Compos. Struct.*, **93**(2), 850-859.
- Toopchi-Nezhad, H. (2014), “Horizontal stiffness solutions for unbonded fiber reinforced elastomeric bearings”, *Struct. Eng. Mech.*, **49**(3), 395-410.
- Tsai, H.C. and Kelly, J.M. (2005), “Buckling load of seismic isolators affected by flexibility of reinforcement”, *Int. J. Solid. Struct.*, **42**(1), 255-269.
- Tsai, H.C. (2007), “Tilting analysis of circular elastic layers interleaving with flexible reinforcements”, *Int. J. Solid. Struct.*, **44**(18-19), 6318-6329.
- Yasser, M.A.A. and Tait, M.J. (2015), “A numerical study on compressive and rotational behavior of fiber reinforced elastomeric isolators (FREI)”, *Compos. Struct.*, **133**, 1249-1266.

CC